

ScienceDirect



IFAC PapersOnLine 55-37 (2022) 107-112

Design for interaction: Factorized Nyquist based control design applied to a Gravitational Wave detector

Mathyn van Dael^{1,3}, Gert Witvoet^{1,2}, Bas Swinkels³, Manuel Pinto⁴, Julia Casanueva⁴, Diego Bersanetti⁵ Maddalena Mantovani⁴, Marco Vardaro³ and Tom Oomen^{1,6}

1 Eindhoven University of Technology, dept. of Mechanical
Engineering, Control Systems Technology
Eindhoven, The Netherlands, email: m.r.v.dael@tue.nl
2 TNO, Optomechatronics Department, Delft, The Netherlands
3 Nikhef, Amsterdam, The Netherlands
4 European Gravitational Observatory (EGO), I-56021 Cascina, Pisa,
Italy

5 INFN, Sezione di Genova, I-16146 Genova, Italy 6 Delft Center for Systems and Control, Delft University of Technology, Delft, The Netherlands

Abstract: Gravitational Wave detectors require feedback control to control the length between the sensitive components of the detector. The degrees of freedom in the control system are inherently coupled and the level of interaction furthermore varies over time. A systematic control design approach for the feedback controllers is presented which provides a guide on how to cope with the varying levels of interaction. A new controller for one of the loops has been designed and experimental results measured on the Gravitational Wave detector Advanced Virgo show a significant reduction in the root mean square error of the loop with the new controller.

Copyright © 2022 The Authors. This is an open access article under the CC BY-NC-ND license (https://creativecommons.org/licenses/by-nc-nd/4.0/)

Keywords: Gravitational Waves, Virgo, Factorized Nyquist, MIMO, Design, Interaction.

1. INTRODUCTION

Control plays a fundamental role in the operation of Gravitational Wave (GW) detectors. GWs are ripples in spacetime that are generated by cosmic events such as the collision of black holes. The first GW was measured in 2015 (Abbott et al., 2016) and many such events have since been detected by GW detectors Advanced Virgo (Acernese et al., 2015) and Advanced LIGO (Aasi et al., 2015). These detectors employ large-scale interferometry to measure the spatial distortions induced by GWs, which are in the order of 10×10^{-18} m for Advanced Virgo. The interferometers consist of many sensitive mirrors which need to be longitudinally controlled with respect to each other, some of which are 3 km apart. The required stability in length between the mirrors is very stringent and feedback control is therefore used to satisfy these requirements. The longitudinal Degrees of Freedom (DoFs), which are the distances between the mirrors, are inherently coupled and the level of coupling also varies over time. The problem addressed in this paper is the redesign of one of the longitudinal control loops, which requires a lower Root Mean Square (RMS) error. Given the inherent interaction between the loops, a MIMO design approach is required to guarantee stability and performance.

This design approach requires a certain level of flexibility as the operating conditions of a GW detector regularly change in certain phases of the operation. Basic databased design tools for MIMO problems such as SISO control design with MIMO stability analysis through the MIMO Nyquist criterion (Desoer and Wang, 1980; van Dael et al., 2022) or Sequential Loop Closing (Loh et al., 1993) are often sufficient for MIMO control problems, but for this particular problem do not provide a clear guide on how to cope with the changing levels of interaction. More elaborate tools such as the Robust Control framework can cope with the changing levels of interaction by analyzing for which set of interaction terms (the uncertainty set) the system is stable (Doyle, 1987) or synthesize a controller for the uncertainty set (Oomen et al., 2014). This framework does however not provide much flexibility due to the significant modelling effort, as the attainable performance depends on the quality of the models.

The aim of this paper is to develop a systematic control design approach that addresses the changing levels of interaction in longitudinally controlling the mirrors of a GW detector. The Factorized Nyquist criterion is proposed as a design tool as this is a data-based method that provides for this particular problem a clear design guide on how to cope with the changing levels of interaction. One of the main contributions of this paper is furthermore to use advancements from the motion control community

 $^{^{1}\,}$ This work has been funded by the Netherlands Organisation for Scientific Research (NWO) under grant number 680.92.18.02.

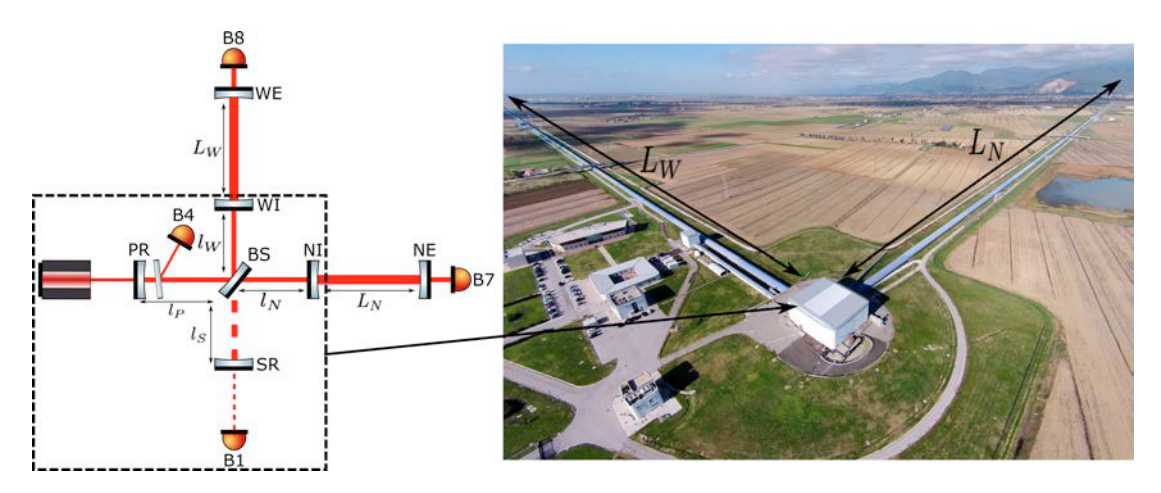


Fig. 1. Part of the optical configuration of Advanced Virgo for the next science run (left) and picture of Advanced Virgo (right). The B1 photodiode measures the interference pattern between the two arms $(l_W + L_W)$ and $l_N + l_N$, which change in length with opposite signs when a GW passes. The two tunnels with length L_W and L_N are 3 km long.

to yield a better control performance in GW detectors. Based on the developed approach, the controller for the longitudinal DoF has been redesigned and experimental results on a GW detector will be presented to illustrate the increase in performance.

The outline of this paper is as follows. In Section 2, an overview of the Advanced Virgo detector will be given and the control problem is formulated. An interaction analysis is then carried out in Section 3 which formalizes the design problem, after which the systematic design approach and new control design based on this approach are presented in Section 4. Experimental results from Advanced Virgo are then presented in Section 5 followed by the conclusions in Section 6.

2. PROBLEM FORMULATION

This section will explain the working principle of the GW detector Advanced Virgo, after which the control problem considered in this paper is delineated.

2.1 System description

Gravitational Wave detectors monitor the interference pattern of two beams of light to detect the passing of a GW. GWs stretch space in one direction and contract it in the orthogonal direction, which increases the length of one of the beams and decreases the length of the other, hence changing the interference pattern. In Fig. 1, the optical configuration of Advanced Virgo for the next science run is depicted. A laser (left) creates a beam of light that is split into two orthogonal directions (upwards and to the right) by the Beam Splitter (BS). The beams travel 3 km through the two arms $(l_W + L_W)$ and $l_N + L_N)$ and are reflected back by the end mirrors (WE and NE) to interfere again at the BS. This interference pattern, a function of the length difference between these two arms, is measured by the B1 photodiode. Additional mirrors are present (PR, SR, WI and NI) to further enhance the signal quality and the lengths between these mirrors need to be controlled with microscopic precision to maximize the detector sensitivity. In Advanced Virgo, the following longitudinal DoFs are controlled

$$L_{\text{DARM}} = L_N - L_W,$$

$$L_{\text{MICH}} = l_N - l_W,$$

$$L_{\text{CARM}} = \frac{L_N + L_W}{2},$$

$$L_{\text{PRCL}} = l_P + \frac{l_N + l_W}{2},$$

$$L_{\text{SRCL}} = l_S + \frac{l_N + l_W}{2},$$
(1)

where DARM stands for Differential Arm length, CARM for Common Arm length, MICH for Michelson, PRCL for Power Recycling Cavity Length and SRCL for Signal Recycling Cavity Length. The DARM and CARM DoFs control the length of the two arms (L_N, L_W) which are in Advanced Virgo 3km long. These two lengths are the most important DoFs as DARM contains the GW signal, while the other three DoFs (MICH, PRCL, SRCL) serve as auxiliary DoFs that further enhance the detector sensitivity. There is a sixth DoF which is the common motion of all mirrors, but this one is not controlled as it does not affect the sensitivity of the detector. The feedback system of the longitudinal DoFs uses actuators on the mirrors to correct the mirror positions, whereas photodiodes at specific locations in the detector are used to derive a relative measure of the length of the DoFs through the Pound-Drever-Hall (PDH) method (see Black (2001) for a full overview of this method).

The controller for SRCL will be redesigned in this paper in order to achieve a lower RMS error in the SRCL loop. Because of the coupling with the MICH and PRCL DoFs, the interaction with these two loops will also be considered in the control design approach. The DARM and CARM DoFs are sufficiently decoupled for them to be neglected in the design.

2.2 Control problem

The block diagram of the control problem for MICH, PRCL and SRCL is depicted in Fig. 2. The feedback controller $K \in \mathbb{R}^{3\times 3}$ uses an error signal

$$e_{\text{arm}} = \left[e_{\text{MICH}} e_{\text{PRCL}} e_{\text{SRCL}}\right]^T$$
 (2)

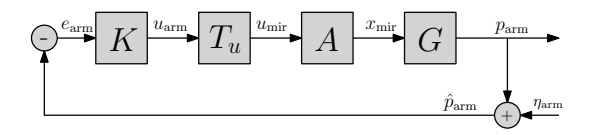


Fig. 2. Block diagram of the control problem for the MICH, PRCL and SRCL DoFs.

to generate a control signal $u \in \mathbb{R}^3$ for each of the DoFs. The matrix $T_u \in \mathbb{R}^{3\times 3}$ applies a coordinate transformation for this actuation signal to obtain an actuation signal

$$u_{\min} = \left[u_{\text{BS}} \ u_{\text{PR}} \ u_{\text{SR}} \right]^T \tag{3}$$

for the BS, PR and SR mirrors. The transfer matrix $A \in \mathbb{R}^{3\times 3}$, representing the electromechanical dynamics of the actuator and mirror, then transforms the actuation signal to a displacement of the mirrors, denoted by $x_{mir} \in \mathbb{R}^3$. The output of the system is the PDH signal based on the photodiode powers, denoted by

$$p_{arm} = \left[p_{\text{MICH}} \, p_{\text{PRCL}} \, p_{\text{SRCL}} \right]^T. \tag{4}$$

These signals are related to the individual mirror motions by $G \in \mathcal{R}^{3\times 3}$, which contains the optical dynamics of the interferometer. The output is spoiled by sensor noise $\eta_{arm} \in \mathbb{R}^3$ and this noisy sensor signal is used as the error signal for the feedback loop. The control objective is to reduce the RMS error for the SRCL DoF (e_{SRCL}) and simultaneously be robust against the varying levels of interaction in G.

3. INTERACTION ANALYSIS

An analysis of the interaction between MICH, PRCL and SRCL will be presented in this section. The Frequency Response Function (FRF) measurements of the plant are first presented together with an analysis of the underlying dynamics, after which an analysis of the interaction and how it varies over time is presented.

3.1 Measurement of the plant

To determine the variation of the interaction over time, three different FRF measurements of the plant were taken with intervals larger than two weeks. The plant of the system is given by

$$H = G \cdot A \cdot T_u \tag{5}$$

and has been identified by exciting the DoFs consecutively with bandpass filtered white noise. The excitation is restricted to the 10 to 100 Hz range in order to not excite the suspension and flexible modes outside this frequency range, which induce very large transients. The magnitudes of the three FRFs of H are depicted in Fig. 3, which shows that all terms in H exhibit roughly the same dynamics between 10 and 100 Hz. The dynamics of each term $h_{n,m}$ in H can be described by

$$h_{n,m}(s) = a_{\text{vc}}(s) \cdot a_{\text{SUSD}}(s) \cdot e^{-s\tau} \cdot \mathcal{H}_{n,m}, \tag{6}$$

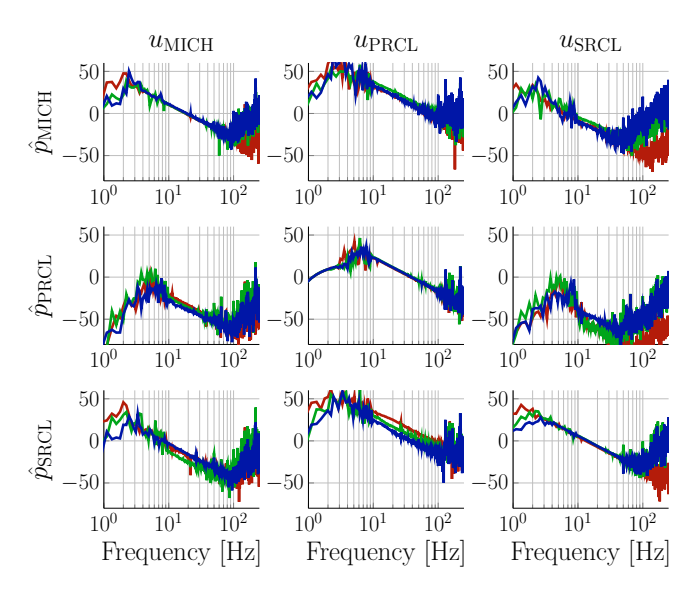


Fig. 3. Magnitude of three different FRF measurements of H, measured at least two weeks apart.

with $\mathcal{H} \in \mathbb{R}^{3\times3}$ the gain of each entry. The first term $a_{\rm vc}$ represents the actuator (voice coil) dynamics, which translates the voltage on the actuators to a force on the mirrors. This can be modelled as a harmonic oscillator with an eigenfrequency at roughly 300 Hz. The transfer function $a_{\rm susp}$ represents the dynamics of the mirrors, i.e. the corresponding mirror motion as a result of the actuator force. This can also be modelled as a harmonic oscillator with an eigenfrequency around 0.5 Hz as the mirrors are suspended with a very low stiffness to isolate ground motion. $a_{\rm susp}$ can thus be approximated by a -2 slope in the 10 to 100 Hz region. There is furthermore a non-negligible delay τ in the system and it is roughly identical for all DoFs. H can therefore be approximated by

$$H(j\omega) \approx h(j\omega) \cdot \mathcal{H} \ \forall \omega \in 2\pi [10\ 100].$$
 (7)

This simplification of the system dynamics will prove useful in the design approach.

3.2 Theory of RGA

The Relative Gain Array (RGA) (Bristol, 1966) will be used to analyze the interaction because of its frequency domain interpretation of interaction. Consider an arbitrary plant $H \in \mathbb{R}^{n \times n}$, the RGA is then defined as

$$\Lambda(j\omega) = H(j\omega) \odot (H(j\omega)^{-1})^T, \tag{8}$$

where \odot denotes the Hadamard product (element wise product). The system is fully decoupled if

$$\Lambda(j\omega) = I_n \,\forall \, \omega, \tag{9}$$

if the diagonal terms of the plant are used to control the output of the system, which is the case for the considered control problem. The off-diagonal terms in $\Lambda(j\omega)$ provide a relative measure of the coupling between the DoFs and can be used as a figure of merit to decide whether SISO design is justified or if MIMO design and stability should be considered.

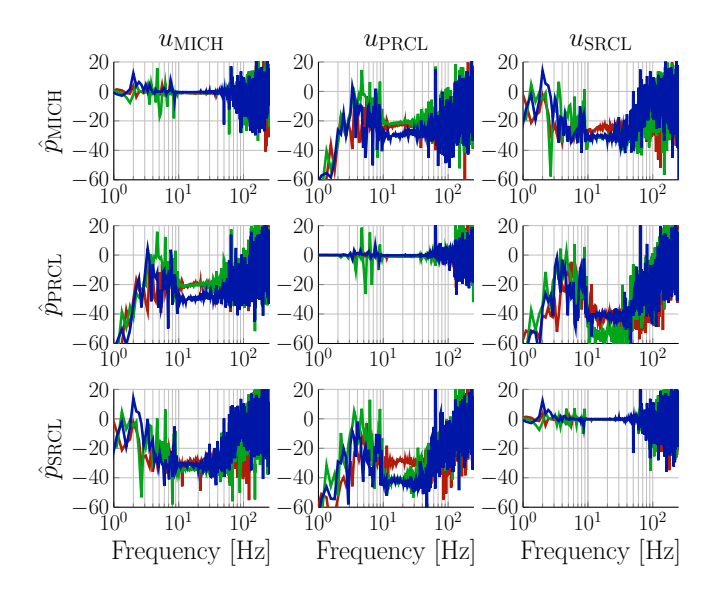


Fig. 4. RGA of three different FRF measurements of H.

3.3 System interaction

The RGA for the three FRFs is depicted in Fig. 4. While the off-diagonal terms are relatively noisy due to poor estimates of H in some of the off-diagonal terms, it is still evident that the coupling between the DoFs is nonnegligible as the RGA is in the order of 0.1 between 10 to 40 Hz. Furthermore, substituting the approximation of H from (7) in the RGA in (8) shows that

$$\Lambda(j\omega) = \lambda \in \mathbb{R}^{3\times3} \ \forall \, \omega \in 2\pi \, [10 \, 100] \,, \tag{10}$$

implying that the interaction is constant between 10 and 100 Hz. This is indeed confirmed by Fig. 4 at the frequencies where all entries of $H(j\omega)$ have sufficiently high coherence (between 10 and 40 Hz).

The coupling between the DoFs is non-negligible and furthermore varies over time. This variation can be explained by the fact that the photodiodes measure a linear combination of the powers in the different DoFs, which are a function of the alignment of the mirrors and thermal aberrations. A control design should therefore be made that is robust against variations in this coupling.

4. DESIGN FOR INTERACTION

In the first part of this section, the use of decoupling to reduce the interaction will be discussed and why it was decided not to use this tool. The new design approach is then discussed after which a new SRCL control design based on this new design approach is presented.

4.1 Decoupling

Static decoupling is typically the first step in a control design to obtain a sufficiently decoupled plant on which SISO control design can be applied. Given the specific structure of H, a decoupling matrix equal to the inverse of \mathcal{H} could theoretically provide sufficient decoupling in order to justify SISO loop designs. However, considering the unpredictable nature of the variations in the interaction

terms (and hence the decoupling matrix), it was opted to go for a control design that is robust against the varying levels of interaction as this would likely require less effort and design time to achieve satisfactory results.

4.2 Factorized Nyquist criterion

Due to the variations in the operating conditions of a GW detector, a control design approach is required that has a low modelling effort and provides a clear design guide on how to cope with the varying levels of interaction. The Factorized Nyquist criterion satisfies both criteria and will therefore be used as a design tool to redesign the SRCL controller. A brief derivation of the criterion is given next and the reader is referred to Grosdidier and Morari (1986) for the full derivation and analysis.

To mathematically derive the design criterion, consider an arbitrary system $H \in \mathbb{R}^{n \times n}$ of which the diagonal terms are defined as

$$\tilde{H} = \operatorname{diag}(H^{ii}) \tag{11}$$

and the normalized off-diagonal terms are denoted by

$$E = \left(H - \tilde{H}\right)\tilde{H}^{-1} \tag{12}$$

such that

$$H = (I + E)\tilde{H}. (13)$$

The return difference matrix can then be rewritten to

$$I + HK = I + (I + E)\tilde{H}K = (I + E\tilde{T})(I + \tilde{H}K),$$
 (14)

with

$$\tilde{T} = \tilde{H}K \left(I + \tilde{H}K \right)^{-1} \tag{15}$$

the complementary sensitivity of the diagonal terms. Taking the inverse of (14) yields

$$(I + HK)^{-1} = \underbrace{(I + \tilde{H}K)^{-1}}_{\tilde{S}} \underbrace{(I + E\tilde{T})^{-1}}_{\text{interaction}}.$$
 (16)

The first term on the right-hand side is the sensitivity of the diagonal terms and the second term represents the interaction. For the system to be MIMO stable, both terms should be individually stable, which the sensitivity of the diagonal terms is by design. Note furthermore that the interaction term consists of a part that only depends on the plant (E) and a part that depends on the controller (\tilde{T}) . A design criterion for the controller can then be derived using the small-gain theorem (Zames, 1966), i.e. the interaction term is stable if

$$I + E(j\omega)\tilde{T}(j\omega) > 0 \,\forall \,\omega,\tag{17}$$

from which it follows that

$$\bar{\sigma}(E(j\omega)\tilde{T}(j\omega)) < 1 \,\forall \,\omega,$$
 (18)

where $\bar{\sigma}$ denotes the maximum singular value. The controllers should therefore be designed such that

$$\bar{\sigma}(\tilde{T}(j\omega)) < \bar{\sigma}^{-1}(E(j\omega)) \,\forall \,\omega.$$
 (19)

The bound $\bar{\sigma}(E(j\omega))$ can be further tightened by using the Structured Singular Value (SSV), see (Packard and Doyle, 1993), which explicitly considers the structure of \tilde{T} when computing the maximum gain of E. The bound in (19) can then be rewritten to

$$\tilde{T}^{ii}(j\omega) < \mu_{\tilde{\mathbf{T}}}^{-1}(E(j\omega)) \,\forall \, \omega, i,$$
 (20)

where $\mu_{\tilde{\mathbf{T}}}(E(j\omega))$ denotes the SSV of E with respect to the structure of \tilde{T} . This criterion can be used as a design tool for each of the controllers. By plotting $\tilde{T}^{ii}(j\omega)$ against $\mu_{\tilde{\mathbf{T}}}^{-1}(E(j\omega))$ for each SISO loop, a clear guide is obtained on how to shape the open-loop transfer functions to be robust against the interaction.

4.3 Control design

Based on the Factorized Nyquist criterion, a new controller for SRCL will be designed that is robust against the varying levels of interaction and also reduces the RMS error of the loop.

Given the specific structure of the plant, see (7), the Factorized Nyquist criterion can be simplified. Substituting the approximation of H from (7) in (12) yields

$$E = \left(h(j\omega) \cdot (\mathcal{H} - \tilde{\mathcal{H}})\right) h^{-1}(j\omega)\tilde{\mathcal{H}}^{-1} = \left(\mathcal{H} - \tilde{\mathcal{H}}\right) \tilde{\mathcal{H}}^{-1},$$
(21)

which shows that E and therefore also $\mu_{\tilde{\mathbf{T}}}(E(j\omega))$ are frequency independent given the specific structure of H. This has the advantage that $\mu_{\tilde{\mathbf{T}}}(E(j\omega))$ only has to be calculated at a few frequency bins where the off-diagonal terms are accurately identified in order to obtain a bound for $\tilde{T}^{ii}(j\omega)$ between 10 and 100 Hz. The SSV can thus be approximated by

$$\mu_{\tilde{\mathbf{T}}}(E(j\omega)) = \alpha \ \forall \, \omega \in 2\pi \, [10 \, 100] \,. \tag{22}$$

The SRCL loop, of which the complementary sensitivity is denoted by $\tilde{T}^{33}(j\omega)$, then has to satisfy

$$\|\tilde{T}^{33}(j\omega)\|_{\infty} < \alpha^{-1}, \tag{23}$$

which can be evaluated for α of all three FRFs. So in order to be robust against the varying levels of interaction, the peak value of the complementary should be sufficiently low, which can be achieved by having sufficient modulus margin in the control design.

Based on the derived design criterion, a new controller has been designed that satisfies (23) for all three FRFs and simultaneously adds gain on the frequency bins where the error spectrum is high, see Fig. 5. The bandwidth of the

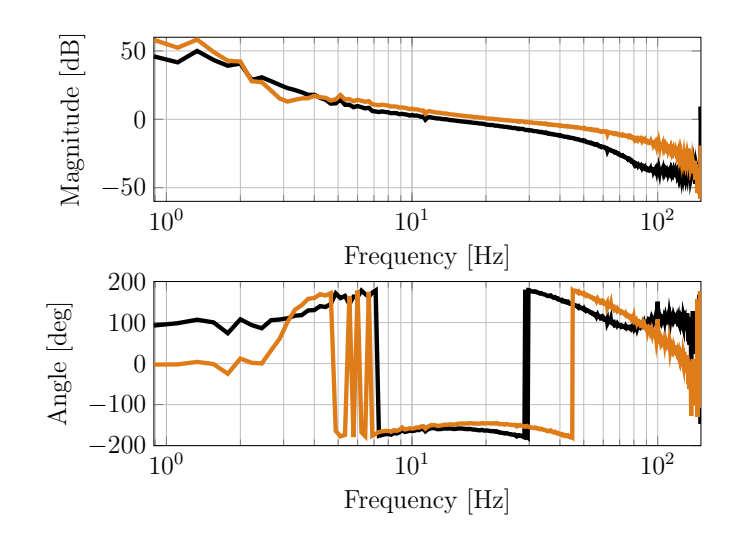


Fig. 5. Bode plot of the open-loop of the old (—) and new (—) SRCL controller.

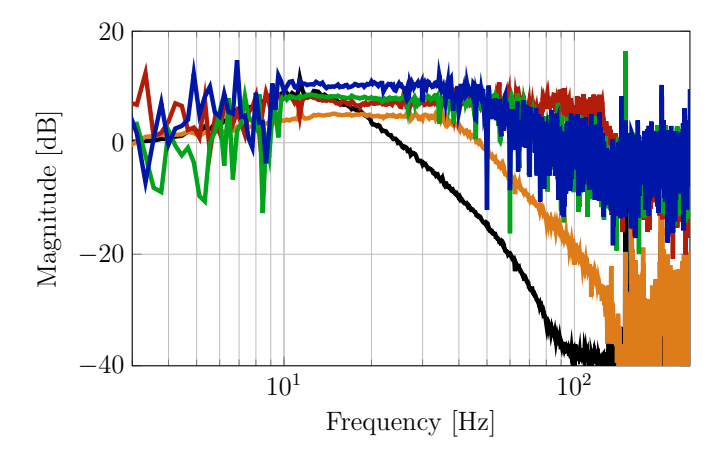


Fig. 6. Stability and robustness assessment using the Factorized Nyquist criterion. (—), (—) and (—) represent $\mu_{\tilde{\mathbf{T}}}^{-1}(E(j\omega))$ computed for the three FRFs. $\tilde{T}^{33}(j\omega)$ is represented by (—) for the old and (—) for the new SRCL controller.

controller has therefore been slightly increased to obtain sufficient gain at low frequencies and the modulus margin has been decreased from roughly 9 dB to 6 dB to satisfy (23). This goes at the expense of the roll-off above the bandwidth, but based on typical error spectra, this is not expected to pose limitations on the attainable RMS.

The design criterion from (23) for the old and new SRCL controller is shown in Fig. 6 together with $\mu_{\tilde{\mathbf{T}}}(E(j\omega))$ of the three FRFs. The old controller for SRCL violates the condition from (23) and while this does not necessarily mean that the system is MIMO unstable (the Factorized Nyquist criterion is only a sufficient condition), the controller will likely not be very robust against the interaction with the other DoFs. The new controller does satisfy the criterion from (23) and some margin is left between the worst case α and $\tilde{T}^{33}(j\omega)$ for robustness purposes.

5. EXPERIMENTAL RESULTS

This section will present experimental results obtained during the commissioning of Advanced Virgo using the

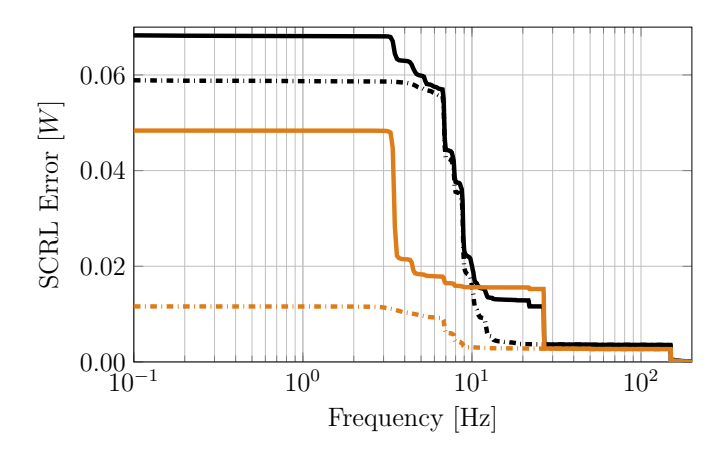


Fig. 7. Cumulative RMS integrated from right to left for the old (—) and new (—) controller. The dashed lines are the same spectra but with some of the calibration lines manually removed.

old and new SRCL controller. The error spectra were obtained by consecutively enabling the two controllers in order to have comparable disturbances. In Fig. 7, the cumulative RMS of e_{SRCL} is depicted by the thick lines for the two controllers. These spectra were obtained during a time when calibration lines were used to monitor certain parameters of the detector and these lines spoil the measured RMS error. To get a more accurate representation, the lines that will be turned off once the detector starts measuring GWs were also manually removed in the measured spectra. The dash-dotted lines represent the spectra with these calibration lines removed, illustrating roughly a factor 5 improvement in RMS. This improvement is mainly achieved in the 5 to 20 Hz range where the gain of the loop was increased. The spectra of the MICH and PRCL loops were also compared with the old and new SRCL controller and the new SRCL controller did not spoil the performance of either of these two loops.

6. CONCLUSION

A systematic control design approach has been presented in this paper for some of the longitudinal DoFs in a GW detector. This design approach provides a guide on how to shape the controllers for robustness against the varying levels of interaction between the longitudinal DoFs and simultaneously improve the loop performance. Based on the presented design approach, the controller for the SRCL DoF was redesigned to achieve a lower RMS error and be robust against the varying levels of interaction. Experimental results on the GW detector Advanced Virgo show a significant reduction in the RMS error using the new controller with respect to the old controller.

ACKNOWLEDGEMENTS

The authors gratefully acknowledge the contributions made by the ISC team at Advanced Virgo for helping to perform the experiments on the interferometer as well as providing the necessary information and support to conduct this work. The authors also gratefully acknowledge the Italian Istituto Nazionale di Fisica Nucleare (INFN), the French Centre National de la Recherche Scientifique (CNRS) and the Netherlands Organization for

Scientific Research, for the construction and operation of the Virgo detector and the creation and support of the EGO consortium. The authors also gratefully acknowledge research support from these agencies as well as by the Spanish Agencia Estatal de Investigación, the Consellera d'Innovació, Universitats, Ciència i Societat Digital de la Generalitat Valenciana and the CERCA Programme Generalitat de Catalunya, Spain, the National Science Centre of Poland and the Foundation for Polish Science (FNP), the European Commission, the Hungarian Scientific Research Fund (OTKA), the French Lyon Institute of Origins (LIO), the Belgian Fonds de la Recherche Scientifique (FRS-FNRS), Actions de Recherche Concertées (ARC) and Fonds Wetenschappelijk Onderzoek – Vlaanderen (FWO), Belgium.

REFERENCES

Aasi, J. et al. (2015). Advanced LIGO. Classical and Quantum Gravity, 32(7), 074001.

Abbott, B.P. et al. (2016). Observation of gravitational waves from a binary black hole merger. *Phys. Rev. Lett.*, 116, 061102.

Acernese, F. et al. (2015). Advanced Virgo: a second-generation interferometric gravitational wave detector. *Class. Quant. Grav.*, 32(2), 024001.

Black, E.D. (2001). An introduction to pound-dreverhall laser frequency stabilization. *American Journal of Physics*, 69, 79–87.

Bristol, E. (1966). On a new measure of interaction for multivariable process control. *IEEE Transactions on Automatic Control*, 11(1), 133–134.

Desoer, C. and Wang, Y.T. (1980). On the generalized nyquist stability criterion. *IEEE Transactions on Automatic Control*, 25(2), 187–196.

Doyle, J. (1987). A review of μ for case studies in robust control. IFAC Proceedings Volumes, 20(5, Part 8), 365–372. 10th Triennial IFAC Congress on Automatic Control - 1987 Volume VIII, Munich, Germany, 27-31 July.

Grosdidier, P. and Morari, M. (1986). Interaction measures for systems under decentralized control. *Automatica*, 22(3), 309–319.

Loh, A.P., Hang, C.C., Quek, C.K., and Vasnani, V.U. (1993). Autotuning of multiloop proportional-integral controllers using relay feedback. *Industrial & Engineer*ing Chemistry Research, 32(6), 1102–1107.

Oomen, T., van Herpen, R., Quist, S., van de Wal, M., Bosgra, O., and Steinbuch, M. (2014). Connecting system identification and robust control for next-generation motion control of a wafer stage. *IEEE Transactions on Control Systems Technology*, 22(1), 102–118.

Packard, A. and Doyle, J. (1993). The complex structured singular value. *Automatica*, 29(1), 71–109.

van Dael, M., Witvoet, G., Swinkels, B., and Oomen, T. (2022). Systematic feedback control design for scattered light noise mitigation in virgo's multisas. In 2022 IEEE 17th International Conference on Advanced Motion Control (AMC), 300–305.

Zames, G. (1966). On the input-output stability of timevarying nonlinear feedback systems part one: Conditions derived using concepts of loop gain, conicity, and positivity. *IEEE Transactions on Automatic Control*, 11(2), 228–238.